Philosophical Magazine, 2014
Vol. 94, No. 5, 464–475, http://dx.doi.org/10.1080/14786435.2013.856525

First-principles density functional theory study of generalized stacking faults in TiN and MgO

S.K. Yadav[a,b], X.-Y. Liu[a]*, J. Wang[a], R. Ramprasad[b], A. Misra[c] and R.G. Hoagland[a]

[a]*Materials Science Technology Division, MST-8, Los Alamos National Laboratory, Los Alamos, NM 87545, USA;* [b]*Materials Science and Engineering, University of Connecticut, Storrs, CT 06269, USA;* [c]*Materials Physics and Applications Division, MPA-CINT, Los Alamos National Laboratory, Los Alamos, NM 87545, USA*

(*Received 10 April 2013; accepted 11 October 2013*)

In this paper, the generalized stacking fault (GSF) energies in different slip planes of TiN and MgO are calculated using highly reliable first-principles density functional theory (DFT) calculations. During DFT calculations, the issue of different ways to calculate the GSF energetics in ceramic materials containing more than one element was addressed and applied. For $\langle 1\,1\,0\rangle/\{1\,1\,1\}$ slip, a splitting of saddle point in TiN was observed. For $\langle 1\,1\,2\rangle/\{1\,1\,1\}$ slip, a stable stacking fault at $a_0/3\langle 1\,1\,2\rangle$ displacement was formed in TiN. For synchroshear mechanism where the slip was accompanied by a cooperative motion of the interfacial nitrogen atoms within the slip plane, a second stable stacking fault was formed at $a_0/6\langle 1\,1\,2\rangle$ displacement. The energy barrier for the shuffling of nitrogen atoms from one state to another is calculated to be 0.70 eV per atom. In contrast, such features are absent in MgO. These differences highlight the influence of complex bonding nature (mixed covalent, ionic, and metallic bondings) of TiN, which is substantially different than that in MgO (simple ionic bonding) on GSF shapes.

Keywords: DFT; ceramic; generalized stacking fault energy; slip; bonding

1. Introduction

Titanium nitride (TiN) is a very hard (with typical hardness ranging from 17.3 to 23.8 GPa [1]) ceramic material, yet electrically conductive (room temperature resistivity of 1.8×10^{-7} Ωm [2]). For bulk TiN, the material is brittle at temperatures below 750 °C [3]. This might suggest that there is little or no dislocation activity in TiN below such temperature. However, experimentally, significant dislocation activities were observed at room temperature in Ti–TiN multilayer specimens for which TiN layer is 150 nm in thickness [4]. In recent years, multilayered nanocomposites made of TiN and Al have been used to explore the effect of layer thickness on hardness and flow strength [5]. It was found that at layer thickness of less than 5 nm, a high flow strength of 4.5 GPa and a high compressive deformability (5–7% plastic strain) are obtained in such layered composites. Understanding dislocation slip across Al/TiN interface as well as through TiN bulk is important to help interpret the experimental phenomena. To this

*Corresponding author. Email: xyliu@lanl.gov

end, to provide measures of the resistance to glide of dislocations in TiN, we have calculated the generalized stacking fault (GSF) energies in different slip planes of TiN.

TiN has a rock-salt (B1) crystal structure with mixed covalent, ionic and metallic bondings. By comparison, MgO with the same crystal structure has simple ionic bonding. Density functional theory (DFT) calculations of GSF energies in such multi-component ceramics have been rare in the past. Only recently, some attempts have been made to calculate the GSF energies in MgO [6,7] using DFT. In the late nineties, Harris and Bristowe [8,9] also calculated the GSF energies in TiC_x, based on empirical tight binding approach. TiC also adopts the rock-salt structure over a wide range of stoichiometries.

In this paper, using accurate *ab initio* DFT calculations, the GSF energies in different slip planes of both TiN and MgO are systematically studied. Interesting features are discovered for the GSF energies in TiN and are reported for the first time here. Subsequently, we compare the DFT results for TiN with the GSF energies in MgO. Finally, we conclude with a summary.

2. The methods

Our DFT calculations were performed using the Vienna *Ab initio* Simulation Package (VASP) [10,11], employing the Perdew, Burke and Ernzerhof (PBE) [12] exchange-correlation functional and the projector-augmented wave methodology [13]. For slab calculations, a $7 \times 7 \times 1$ Monkhorst–Pack mesh for k-point sampling and a plane wave cut-off of 500 eV for the plane wave expansion of the wave functions were used. Table 1 shows excellent agreement between the present results and previous (calculated and experimental) values of lattice parameters, bulk modulus and elastic constants of MgO and TiN in rock-salt crystal structure [14–17].

The concept of GSF energy was introduced by Vitek [18] about 40 years ago. GSF energy represents the extra energy needed for a rigid shear displacement at a given glide plane. It can be incorporated into Peierls–Nabarro models to calculate the core properties of dislocations, and to determine the Peierls stress of dislocations. GSF energy provides a useful measure of the resistance to glide of dislocations, and

Table 1. Comparison of calculated and experimental values of lattice parameters, bulk modulus and elastic constants of MgO and TiN. The experimental data are obtained at room temperature.

	MgO		TiN	
	Calc.	Expt.	Calc.	Expt.
Lattice paramter (Å)	4.25	4.21[a]	4.24	4.24[c]
Bulk modulus (GPa)	163	162[b]	277	288[d]
C_{11} (GPa)	269	297[b]	639	625[e]
C_{12} (GPa)	93	95[b]	139	165[e]
C_{44} (GPa)	146	156[b]	160	163[e]

[a]Ref. [38].
[b]Ref. [14].
[c]Ref. [15].
[d]Ref. [37].
[e]Ref. [36].

also for nucleation of dislocations [19,20]. GSF energy is also useful in identifying likely and unlikely dislocation dissociation reactions by distinguishing stable and unstable stacking faults. In the original approach, GSF energy is the excess energy per unit area, calculated by imposing a rigid shear displacement between two neighbouring layers of atoms, except that all atoms are allowed to relax in the directions perpendicular to the shear displacement direction.

We calculated the GSF energies of TiN and MgO on {1 0 0}, {1 1 0} and {1 1 1} planes along the $\langle 1\,\bar{1}\,0\rangle$ direction and on {1 1 1} planes along the $\langle 1\,1\,\bar{2}\rangle$ direction. Supercell set-ups for {1 0 0}, {1 1 0} and {1 1 1} slip planes are shown in Figure 1. We considered a slab with vacuum on either side and the thickness of the slab (30–40 Å) is sufficient so that both free surfaces have negligible influences on results. Both {1 0 0} and {1 1 0} surface-terminated slabs are stoichiometric in nature, hence symmetric, while in the case of {1 1 1} surface-terminated slabs, the surfaces were arranged to be terminated with N atoms to make the slab symmetric. At each applied shear displacement, all the atoms were allowed to relax to a high degree of accuracy, with force on each atom less than 0.03 eV/Å.

For compounds such as TiN and MgO, composed of two elements, we find that the calculation of GSF energies is more complex than for monatomic crystals, especially on {1 1 1} planes. For TiN (and similarly for MgO), examples of methods for calculating GSF energies are schematically shown in Figure 2(a–c), for the case of {1 1 1} plane.

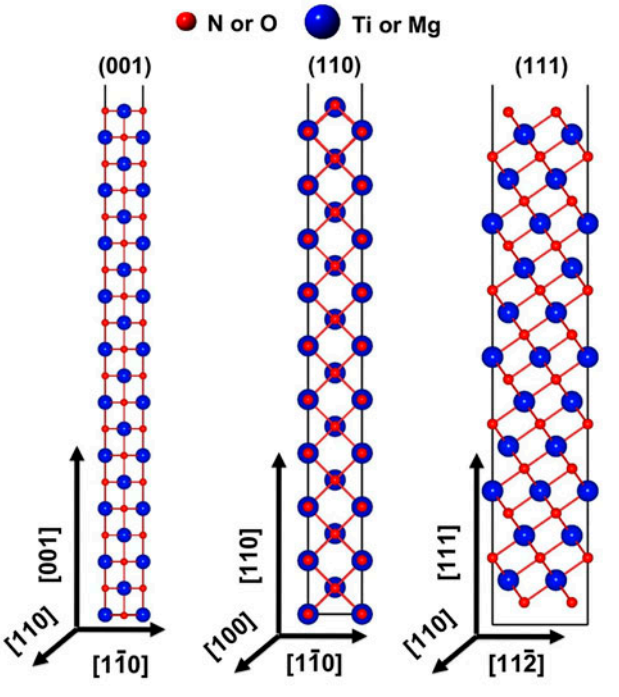

Figure 1. (colour online) Schematic of supercell set-up for different possible slip planes (0 0 1), (1 1 0) and (1 1 1) in TiN and MgO. The blue atom is Ti or Mg, and the red atom is N or O.

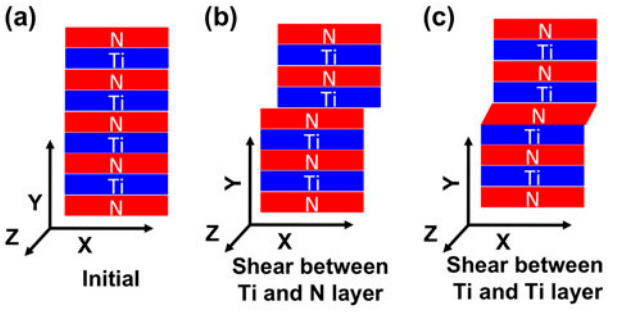

Figure 2. (colour online) Schematic of different ways to calculate the general stacking fault energy in TiN and MgO.

Figure 2(a) represents the initial unsheared structure. In Figure 2(b), the shear displacement is between one Ti layer and its neighbouring N layer. Alternatively, as shown in Figure 2(c), the shear displacement can also be applied between two neighbouring Ti layers at the interface, while allowing the N layer in-between the two Ti layers to relax. The third way to calculate GSF in TiN is to impose the same shear displacement as in Figure 2(c), but with the N atoms in the N layer in-between the two Ti layers be allowed to shift in their positions after the shear displacement. After that the atoms then undergo relaxations. In this scenario, the so-called synchroshear mechanism [21], the slip is accompanied by a cooperative motion of the interfacial nitrogen atoms within the slip plane. So, the N atoms shuffle from one state to another state, overcoming an energy barrier along the path. In our DFT calculations, we have taken all three scenarios into consideration. In addition, we have also considered the effect of allowing the surface atoms to relax in the surface normal direction for all cases in Figure 2(a–c). However, the GSF energy change with and without relaxing surface atoms is found to be insignificant, typically a few percent at most. For all DFT results reported here, the calculations were done with top surface atoms fixed.

3. Results and discussions

3.1. *TiN: displacements along the ⟨1 1 0⟩ direction on {0 0 1}, {1 1 0} and {1 1 1} planes*

In B1 structure, cation and anion atoms sit on two inter-penetrating fcc lattice. The shortest possible Burgers vector for perfect dislocations is $a_0/2\langle 1\,1\,0\rangle$, where a_0 is the lattice constant. We started our GSF energy calculations with shear displacements in the $\langle 1\,1\,0\rangle$ direction in TiN. We considered three low-index shear planes, $\{0\,0\,1\}$, $\{1\,1\,0\}$ and $\{1\,1\,1\}$, as these low-index planes are the most likely slip planes for dislocations in TiN.

The DFT results of GSF energies as a function of shear displacements along the $\langle 1\,1\,0\rangle$ direction in $\{0\,0\,1\}$, $\{1\,1\,0\}$ and $\{1\,1\,1\}$ planes are shown in Figure 3. For both $\{0\,0\,1\}$ and $\{1\,1\,0\}$ planes, there is a single saddle point in the GSF energy curve at the unstable stacking fault. However, this is not true for the $\{1\,1\,1\}$ plane. For $\{1\,1\,1\}$ plane, a 'double hump' with two saddle points exists in the GSF energy curve with the

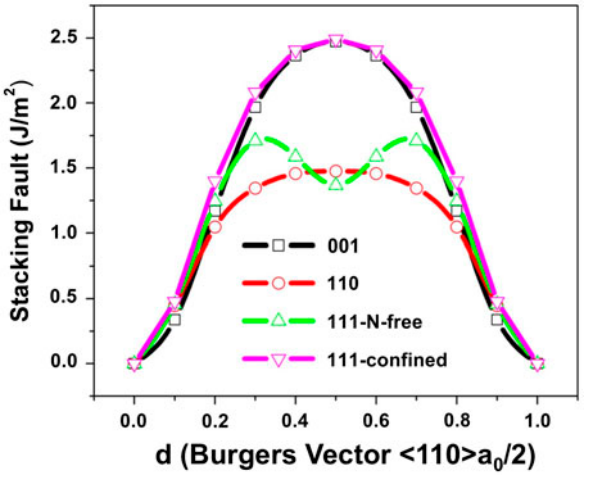

Figure 3. (colour online) The GSF energies as a function of shear displacement along ⟨1 1 0⟩ in {0 0 1}, {1 1 0} and {1 1 1} planes. '1 1 1-N-free': rigid shearing between two Ti layer and N allowed to relax freely in between. '1 1 1-confined': similar to '1 1 1-N-free' but all atoms are allowed to relax in [1 1 1] direction only.

maximum GSF energy of 1.7 J/m^2 at the saddle points. This value is slightly higher than the unstable stacking fault energy in the {1 1 0} plane case (1.48 J/m^2), and is lower than the unstable stacking fault energy in the {0 0 1} plane case (2.47 J/m^2).

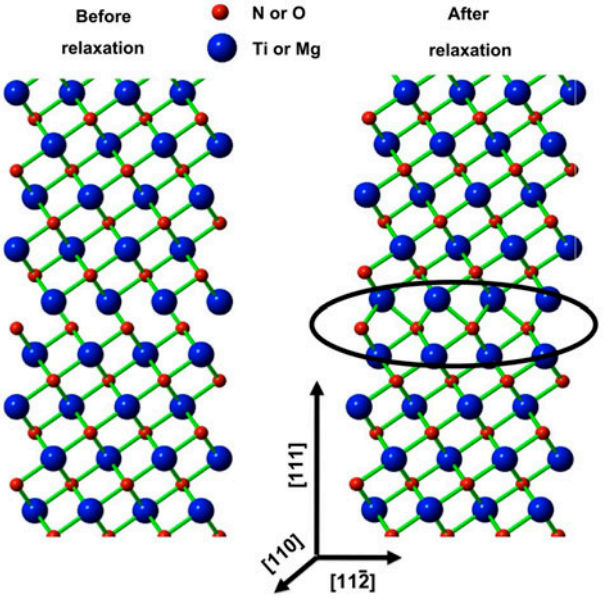

Figure 4. (colour online) The atomic structure before and after relaxation during the calculations of the GSF energy when the shear displacement is $a_0/4\langle 1\,1\,0\rangle$, for the {1 1 1} plane case. The blue atom is Ti, and the red atom is N.

The 'double hump' splitting in the {1 1 1} plane case is interesting. In Figure 4, the atomic structures before and after the structural relaxation when the shear displacement is $a_0/4\langle 1\,1\,0\rangle$ (or c_1), are shown. This displacement is right in the middle of the GSF energy curve corresponding to a maximum for the case of no splitting. As seen in Figure 4, a new structure on the slip plane is formed after the relaxation. The relative shift of the Ti atoms due to the structural relaxation is $a_0/12\langle 1\,\bar{1}\,2\rangle$ (or c_2). The sum of c_1 and c_2 is a Shockley partial vector $a_0/6\langle 2\,1\,1\rangle$. From Figure 4, the new structure at the interface is equivalent to a stacking fault with displacement of a Shockley partial vector in the Ti sublattice. It is noted that the sense of the vector is equivalent to the 'anti-twinning' sense in an fcc metal, which is opposite in direction to the regular Shockley partial vector in the 'twinning' sense. The splitting also suggests the dissociation of $\langle 1\,1\,0\rangle/2$ dislocation into two Shockley partial dislocations in the $\langle 2\,1\,1\rangle$ direction. We calculated the equilibrium distance between the two partials to be 8 Å from isotropic elasticity [22]. To further investigate this, we also applied the shear displacements in the $\langle 1\,1\,2\rangle$ direction on {1 1 1} plane.

3.2. *TiN: displacements along the $\langle 1\,1\,2\rangle$ direction on {1 1 1} plane*

The DFT calculated GSF energy as a function of shear displacements along the $\langle 1\,1\,2\rangle$ direction on {1 1 1} plane is shown in Figure 5. We show three sets of GSF energies using different relaxation criteria, namely (1) 'N-fixed-in-plane': shearing of one N layer with respect to a neighbouring Ti layer at the interface; (2) 'without-N-position-changed': shearing between two Ti layers at the interface, and N atoms in-between are allowed to freely relax; and (3) 'with-N-position-changed': same as (2) but the N atoms in-between the two Ti layers at the interface are allowed to jump (shift in positions) in the [1 1 0]

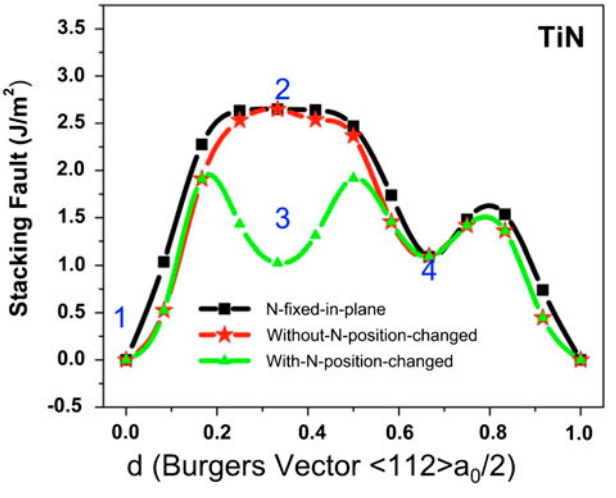

Figure 5. (colour online) The GSF energies as a function of shear displacement along $\langle 1\,1\,2\rangle$ in {1 1 1} plane. 'N-fixed-in-plane': rigid shearing of N layer with respect to Ti layer. 'Without-N-position-changed': rigid shearing between two Ti layer and N allowed to relax freely in between. 'With-N-position-changed': rigid shearing between two Ti layer with N allowed to relax freely in between and shift allowed in [1 1 0] direction.

direction to find minimum energy. From Figure 5, set 1 has the highest energy, since it has the lowest degree of freedom. Set 2 has lower energy compared to set 1, but it maintained the shape of the energy curve in set 1. In contrast, set 3 has the lowest energy among all three sets of results and changed the shape of the energy curve in set 1. The highest energy saddle point in set 1 (and set 2) dropped substantially in energy and split into two saddles, leaving a stable stacking fault. To facilitate discussion of results, in Figure 5, four configurations are marked, (1) the initial configuration with zero displacement; (2) the highest energy saddle point configuration in set 1 and set 2 results, with $a_0/6\langle 1\,1\,2\rangle$ displacement; (3) same displacement as in (2), but a substantially lowered energy as in set 3 result; and (4) with $a_0/3\langle 1\,1\,2\rangle$ in displacement. The atomic arrangements corresponding to four configurations are shown in Figure 6.

Following the notation of Frank and Nicholas [23,24], we label planes of atoms containing Ti by Roman letters and planes of atoms containing N by Greek letters. The stacking sequence of the {1 1 1} planes of TiN can be expressed as … AγBαCβAγBαCβ … In both set 1 and set 2 results, at displacement of $a_0/6\langle 1\,1\,2\rangle$ (configuration 2), which corresponds to a Shockley partial vector, the stacking sequence is changed to … AγBαCβ|BαCβAγ …, where '|' indicates the position of the fault plane. In this configuration, one Ti layer is displaced relative to the neighbouring Ti layer in the 'twinning' sense, resulting in the displaced Ti layer atoms (in 'B' positions) directly on top of N atom (in 'β' positions), with unrelaxed Ti–N bond length of only 1.2 Å. To compare,

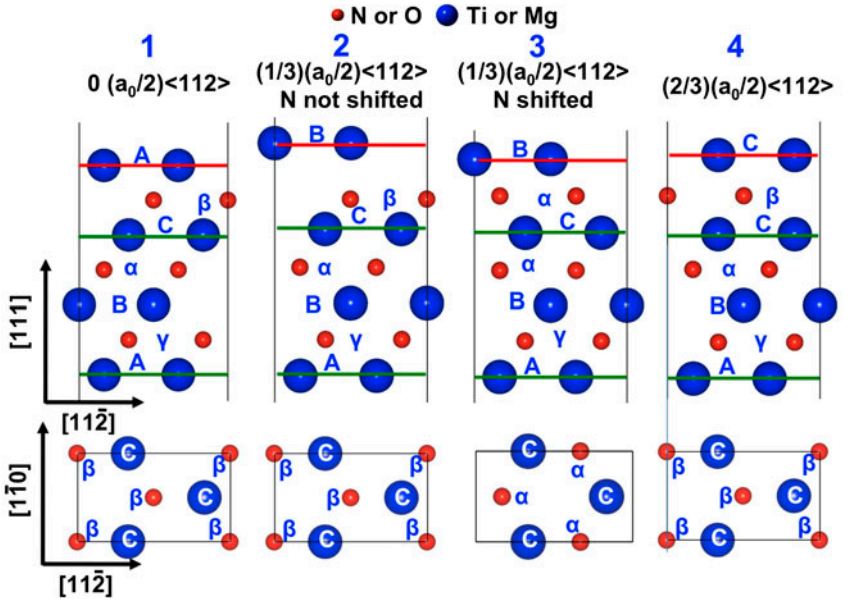

Figure 6. (colour online) The atomic arrangements corresponding to four configurations with different displacements as labeled in Figure 5. Top row shows atomic arrangements with projection along [1 1 0] direction. Bottom row shows the same atomic arrangements with projection along [1 1 1] direction. The blue atom is Ti, and the red atom is N. Atoms bound by green lines are not displaced and the Ti atoms crossed with red line are shear displaced with respect to underlying Ti layer.

the Ti–N bond length in TiN bulk is 2.1 Å. Such a structural arrangement leads to large energy penalty even after structural relaxations.

As depicted in Figure 6, the N atoms at the slip plane can also be 'shifted' from the 'β' position (configuration 2) to 'α' position (configuration 3). In configuration 3, the N atoms at the slip plane are shuffled between the two states, the earlier defined synchroshear mechanism. We carried out the DFT nudged elastic band (NEB) method [25,26] calculations to determine the energy barrier involved in the syschroshear mechanism. The starting configuration is configuration 2 and the final configuration is configuration 3. The energy barrier determined is 0.70 eV per atom. The advantage of the NEB method is that it can detect possible transition states that may involve coupled motions between atoms [27–31]. This magnitude of energy barrier indicates that such mechanism will not be operative at low temperature but could be operative in the intermediate to high temperature range, assuming no other barrier for nucleation. For configuration 3, the stacking sequence is changed to … AγBαC|α|BαCβAγ …

For further displacement, at $a_0/3\langle 1\,1\,2\rangle$, a stable stacking fault is formed (configuration 4) in all three sets of results. This corresponds to a Ti layer at the slip plane displaced by a Shockley partial Burgers vector in the 'anti-twinning' sense. The stacking sequence of {1 1 1} planes is now changed to … AγBαCβ|CβAγBα … In this configuration, the Ti atoms at the slip plane, which are in 'C' positions, are on top of the neighbouring N atoms, which are in 'β' positions. Below this N layer, another layer of Ti atoms are also in 'C' positions. However, such an arrangement does result in a lowest energy local minimum in the displacement paths for all three sets of results. If it were in fcc metals, this would correspond to an energetically unfavourable high energy saddle point.

The above calculations are limited to intrinsic stacking faults. It is also possible to calculate the GSF energies of extrinsic stacking faults. Geometry considerations lead to a conclusion that extrinsic faults should be higher in energies than the intrinsic stacking faults in TiN, therefore such step is omitted in our DFT calculations.

3.3. *MgO: displacements along the ⟨1 1 0⟩ direction on {0 0 1}, {1 1 0} and {1 1 1} planes and along the ⟨1 1 2⟩ direction on {1 1 1} plane*

Next, we compare the DFT calculated GSF energies in MgO with those in TiN. In Figure 7, our DFT calculated GSF energies in MgO along the ⟨1 1 0⟩ direction on the {0 0 1}, {1 1 0} and {1 1 1} planes are shown and compared to the corresponding results in TiN. The trends of GSF energies in TiN and MgO are similar on {0 0 1} and {1 1 0} planes, both indicating a higher Peierls barrier for dislocations on {0 0 1} plane as compared to {1 1 0} plane. For {1 1 1} plane, when shearing of atoms is applied in such a way that all atoms are not allowed to relax in the ⟨1 1 2⟩ direction, then the GSF energy curves are also similar in both TiN and MgO. When relaxation in the ⟨1 1 2⟩ direction is allowed, a similar structure is formed in MgO as in TiN, however, the GSF energy curve in MgO does not show a splitting of the saddle point.

Such influence due to the nature of bonding is also apparent for GSF energies along ⟨1 1 2⟩/{1 1 1} direction, as shown in Figure 8. While there are two stable stacking faults observed in the case of TiN, no such stable stacking faults are found in MgO. At shear displacement of $a_0/6\langle 1\,1\,2\rangle$, the shuffling of O layer atoms at the interface from one state to another state is still energetically preferred in MgO. However, only a

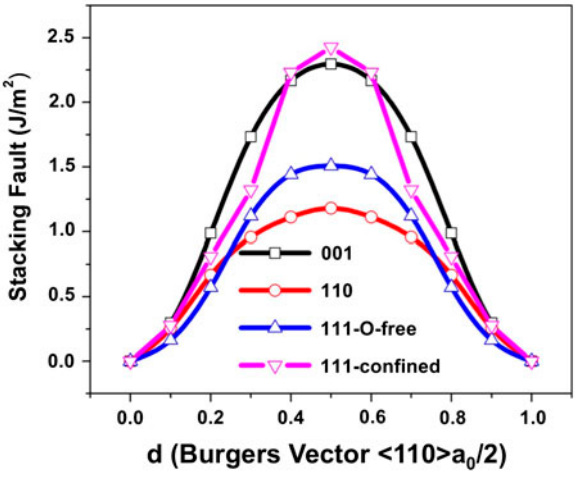

Figure 7. (colour online) MgO: The GSF energies as a function of shear displacement along ⟨1 1 0⟩ on {0 0 1}, {1 1 0} and {1 1 1} planes.

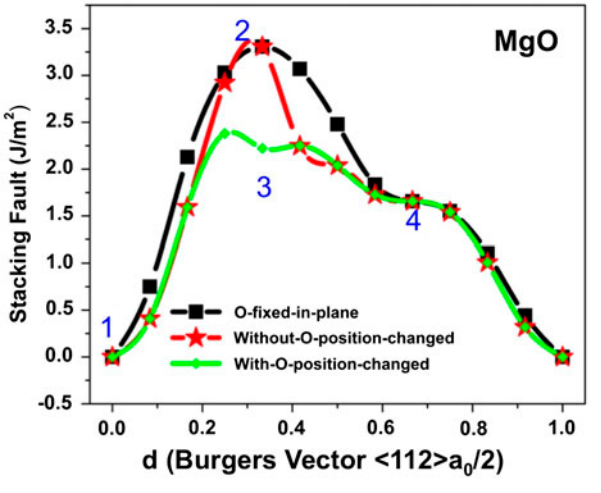

Figure 8. (colour online) MgO: The GSF energies as a function of shear displacement along ⟨1 1 2⟩ in {1 1 1} plane.

metastable stacking fault was formed as a result (see Figure 8). At $a_0/3\langle 1\,1\,2\rangle$ shear displacement, no splitting of saddle point is observed in MgO.

The calculated GSF energies in MgO are in good agreement with previous DFT results [6,7]. Experimentally, it was reported the Peierls stresses for $a_0/2\langle 1\,1\,0\rangle\{1\,1\,0\}$ dislocations in MgO in the range of 60 to 65 MPa for edge dislocations and 86–170 MPa for screw dislocations [32,33]. The critical resolved shear stress (CRSS) in

MgO is about 40 times higher for slip on the {0 0 1} plane compared to that on the {1 1 0} plane at 800 K [34,35]. We found no experimental Peierls stress measurement in TiN. The GSF energy results in MgO indicate the correct order of the importance of dislocation slip planes, {1 1 0} plane followed by {0 0 1} plane. For {1 1 1} slip plane, the trajectory of slip is also possible, which is accompanied by two Shockley partials for the perfect dislocation $a_0/2\langle 1\,1\,0\rangle$. From our DFT results of GSF energies in TiN, accordingly, we expect the order of importance of dislocation slip plane in TiN to be {1 1 0} plane followed by {1 1 1} plane, and {0 0 1} plane is expected to be least important.

4. Summary

In summary, we carried out highly reliable DFT calculations to determine the GSF energies in TiN and MgO for different slip planes and directions of interest. The differences in GSF energies and the shape of the GSF profiles for these two materials highlight the influence of the complex bonding nature (mixed covalent, ionic and metallic bonding) of TiN, which is substantially different from that in MgO (which displays predominantly ionic bonding). The main findings are briefly summarized as below:

(1) For compounds such as TiN and MgO, composed of two elements, we find that the calculation of GSF energies is more complex than in monatomic crystals, especially on {1 1 1} planes.
(2) For $\langle 1\,1\,0\rangle/\{1\,1\,1\}$ slip, a splitting of saddle point in TiN was observed. Such splitting is not observed in MgO.
(3) For $\langle 1\,1\,2\rangle/\{1\,1\,1\}$ slip, a stable stacking fault at $a_0/3\langle 1\,1\,2\rangle$ displacement was formed in TiN, while such stable stacking fault is not observed in MgO.
(4) For synchroshear mechanism where the slip was accompanied by a cooperative motion of the interfacial nitrogen atoms within the slip plane, a second stable stacking fault was formed at $a_0/6\langle 1\,1\,2\rangle$ displacement. The energy barrier for the shuffling of the nitrogen atoms from one state to another is calculated to be 0.70 eV per atom. Such mechanism leading to the formation of stable stacking fault is also missing in MgO.
(5) The calculated GSF energies in MgO indicate the correct order of the importance of dislocation slip planes, {1 1 0} plane followed by {0 0 1} plane. For the {1 1 1} slip plane, the trajectory of slip is also possible, which is accompanied by two Shockley partials for the perfect dislocation $a_0/2\langle 1\,1\,0\rangle$. Accordingly, we expect the order of importance of dislocation slip plane in TiN is {1 1 0} followed by {1 1 1}, and {0 0 1} is least important.

Acknowledgements

This work was supported by the US Department of Energy, Office of Science, Office of Basic Energy Sciences. SKY and XYL also acknowledge partial support by the Los Alamos National Laboratory (LANL) Directed Research and Development Program. LANL is operated by Los Alamos National Security, LLC, for the National Nuclear Security Administration of the US Department of Energy under Contract No. DE-AC52-06NA25396. The authors acknowledge insightful discussions with Prof. J.P. Hirth.

References

[1] H. Ljungcrantz, M. Odén, L. Hultman, J.E. Greene and J.E. Sundgren, J. Appl. Phys. 80 (1996) p.6725.
[2] B.O. Johansson, J.E. Sundgren, J.E. Greene, A. Rockett and S.A. Barnett, J. Vac. Sci. Technol. A 3 (1985) p.303.
[3] T. Yamada, M. Simada and M. Koizumi, Am. Ceram. Soc. Bull. 59 (1980) p.611.
[4] S. Kumar, D.E. Wolfe and M.A. Haque, Int. J. Plasticity. 27 (2011) p.739.
[5] D. Bhattacharyya, N.A. Mara, P. Dickerson, R.G. Hoagland and A. Misra, Acta Mater. 59 (2011) p.3804.
[6] P. Carrez, D. Ferre and P. Cordier, Modelling. Simul. Mater. Sci. Eng. 17 (2009) p.035010.
[7] J. Amodeo, P. Carrez and P. Cordier, Philos. Mag. 92 (2012) p.1523.
[8] R.M. Harris and P.D. Bristowe, Mater. Res. Soc. Symp. Proc. 458 (1997) p.9.
[9] R.M. Harris and P.D. Bristowe, Philos. Mag. 79 (1999) p.705.
[10] G. Kresse and J. Hafner, Phys. Rev. B 47 (1993) p.558.
[11] G. Kresse and J. Furthmüller, J. Comput. Mater. Sci. 6 (1996) p.1516.
[12] J.P. Perdew, K. Burke and M. Ernzerhof, Phys. Rev. Lett. 77 (1996) p.3865.
[13] P.E. Blöchl, Phys. Rev. B 50 (1994) p.17953.
[14] C.S. Zha, H.K. Mao and R.J. Hemley, Proc. Natl. Acad. Sci. U.S.A. 97 (2000) p.13494.
[15] N. Schoenberg, Acta Chem. Scand. 8 (1954) p.213.
[16] M. Marlo and V. Milman, Phys. Rev. B 62 (2000) p.2899.
[17] S.K. Yadav, R. Ramprasad, A. Misra and X.-Y. Liu, J. Appl. Phys. 111 (2012) p.083505.
[18] V. Vitek, Cryst. Lattice Defects 5 (1974) p.1.
[19] J.A. Zimmerman, H.J. Gao and F.F. Abraham, Modelling. Simul: Mater. Sci. Eng. 8 (2000) p.103.
[20] H. Van Swygenhoven, P.M. Derlet and A.G. Froseth, Nature Mater. 3 (2004) p.399.
[21] M.L. Kronberg, Acta Metall. 5 (1957) p.507.
[22] J.P. Hirth and J. Lothe, *Theory of Dislocations*. New York: McGraw-Hill, 1982, Equation 10.14 from.
[23] F.C. Frank and J.F. Nicholas, Philos. Mag. 44 (1953) p.1213.
[24] A. Kelly and D.J. Rowcliffe, Phys. Stat. Sol. 14 (1966) p.K29.
[25] H. Jónsson, G. Mills, K.W. Jacobsen, in *Classical and quantum dynamics in condensed phase simulations*, B.J. Berne, G. Ciccotti and D.F. Coker, eds., World Scientific, Singapore, 1998, p.385.
[26] G. Henkelman, B.P. Uberuaga and H. Jónsson, J. Chem. Phys. 113 (2000) p.9901.
[27] X.-Y. Liu, R.G. Hoagland, J. Wang, T.C. Germann and A. Misra, Acta Mater. 58 (2010) p.4549.
[28] X.-Y. Liu, B.P. Uberuaga, A.D. Andersson, C.R. Stanek and K.E. Sickafus, Appl. Phys. Lett. 98 (2011) p.151902.
[29] X.-Y. Liu, B.P. Uberuaga, M.J. Demkowicz, T.C. Germann, A. Misra and M. Nastasi, Phys. Rev. B 85 (2012) p.012103.
[30] X.-Y. Liu, D.A. Andersson and B.P. Uberuaga, J. of Mater. Sci. 47(21) (2012) p.7367.
[31] K. Kolluri, M.J. Demkowicz, R.G. Hoagland and X.-Y. Liu, JOM 65(3) (2013) p.374.
[32] R.N. Singh and R.L. Coble, J. Appl. Phys. 45 (1974) p.981.
[33] Y. Gaillard, C. Tromas and J. Woirgard, Acta Mater. 54 (2006) p.1409.
[34] T.E. Mitchell and A.H. Heuer, *in Dislocations in Solids*, Ch. 5, F. R. N. Nabarroand J. P. Hirth, eds., Elsevier B.V., 2005, p.339.
[35] P. Haasen, *in Dislocations and Properties of Real Materials*, M.H. Loretto, ed., The Institute of Metals, London, 1985, p.312.

[36] J.O. Kim, J.D. Achenbach, P.B. Mirkarimi, M. Shinn and S.A. Barnett, J. Appl. Phys. 72 (1992) p.1805.
[37] V.A. Gubanov, A.L. Ivanovsky and V.P. Zhukov, *Electronic Structure of Refractory Carbides and Nitrides*, Cambridge University Press, Cambridge, 1994.
[38] R.W.G. Wyckoff, *Crystal Structures*, Wiley, New York, 1964.